Electronic Supplementary Material (ESI) for Journal of Materials Chemistry A.

Understanding the Mechanism of Synthesis of Pt_3Co Intermetallic Nanoparticles via Preferential Chemical Vapor Deposition

Electronic Supporting Information

Saeed Saedy[a,b], Dennis Palagin[b], Olga Safonova[b], Jeroen Anton van Bokhoven[b, c, *], Abbas Ali Khodadadi[a, d], Yadollah Mortazavi[a, d, *]

[a]Catalysis and Nanostructured Materials Laboratory, School of Chemical Engineering, University of Tehran, P.O. Box: 11155/4563, Tehran, Iran.

[b]Laboratory for Catalysis and Sustainable Chemistry, Paul Scherrer Institut, 5232 Villigen, Switzerland.

[c]Institute for Chemistry and Bioengineering, ETH Zurich, Vladimir-Prelog-Weg 1, 8093 Zürich, Switzerland.

[d]Oil and Gas Processing Center of Excellence, School of Chemical Engineering, College of Engineering, University of Tehran, P.O. Box: 11155/4563, Tehran, Iran.

[*]Corresponding authors E-mail addresses:

mortazav@ut.ac.ir (Y. Mortazavi), jeroen.vanbokhoven@chem.ethz.ch (J. A. van Bokhoven)

Table of Contents

Experimental Section

Materials

Cerium(III) nitrate hexahydrate ($Ce(NO_3)_3.6H_2O$ – Sigma-Aldrich) was used as CeO_2 precursor and sodium hydroxide (NaOH – Merck) was used as precipitanting agent. Dihydrogen hexachloroplatinate (IV) hydrate ($H_2PtCl_6.xH_2O$ – Alfa-Aeser) and Cobalt(II) acetylacetonate ($Co(C_5H_7O_2)_2$ – Sigma-Aldrich) were used to deposit platinum and cobalt on CeO_2. All the chemicals were used without further purification.

Synthesis of Cerium Oxide Nanorods

Cerium oxide Nanorods (NRs) were synthesized following the literature procedure.[1] 50 ml of a $Ce(NO_3)_2.6H_2O$ (7.5 m/v %) were mixed with 100 ml NaOH (9 M) in a 200 ml Teflon lined autoclave and stirred for 30 min. The reaction mixture was heated to 100°C for 24 h. After cooling, the obtained solid was suspended in water and centrifuged. The procedure was repeated until the pH of the supernatant was neutral. The obtained solid was dried overnight at 100°C.

Preparation of Pt/CeO_2

Platinum nanoparticles (NPs) were loaded on cerium oxide NRs via incipient wetness impregnation as a simple and efficient method for deposition of monometallic particles on various supports. The uptake capacity of cerium oxide NRs was determined via dropwise adding of Milli-Q water to 1 g of grinded NRs. Platinum salt was dissolved in adequate amount of Milli-Q water and obtained solution was added to grinded CeO_2 NRs dropwise aiming at perfectly wetting of support material without extra liquid. The obtained mixture was dried overnight at room temperature and the remaining moisture was removed via 12 h drying at 100°C.

Preferential chemical vapor deposition of Co on Pt/CeO_2

A homemade setup (Fig. S-1) similar to the ALD/CVD setup reported by Khodadadi and co-workers[2, 3] was used for preferential chemical vapor deposition of $Co(acac)_2$ on Pt/CeO_2. The cobalt precursor was sublimed and carried using argon flow to the deposition zone. The $Co(acac)_2$ vapor was mixed with hydrogen flow and fed to deposition zone. The sublimation and deposition zones were isolated from each other, preventing thermal mixing of zones. Aiming at enhanced transport of species and homogenous cobalt deposition, a reactor with special geometry was designed to feed the mixture of reactants from the bottom of the deposition zone. This configuration makes a bubbling fluidized flow regime, leading to a well-mixed deposition bed.

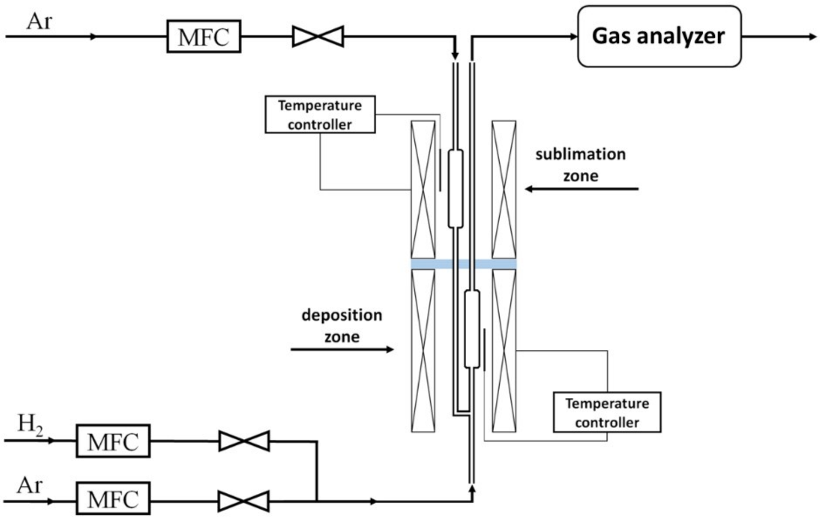

Fig. S-1. Schematic of experimental setup used for preferential chemical vapor deposition of cobalt on platinum. The setup includes 2 independent heating zones of sublimation and deposition, gas flow controlling units, and the CVD reactor.

The temperature window study of $Co(acac)_2$ deposition on CeO_2 and Pt/CeO_2 was conducted using fresh support material for each one of the deposition temperatures used in this study. 1 g of $Co(acac)_2$ was located in the sublimation zone, as well as 0.5 g of the support material in the deposition zone. The as synthesized support materials were pressed, crushed, and sieved to particles in the range of 100 – 180 µm. The CVD reactor was purged using argon flow through both sublimation and deposition zones at room temperature to eliminate oxygen. The temperature of deposition zone was set to the desired temperature with heating rate of 5 °C/min; during heating course of deposition zone a flow of 60 ml/min of Ar and H_2 mixture (50% H_2 and 50% Ar) was passed through the deposition zone. The support material was treated by 50% hydrogen in Ar flow for 1 h. Meanwhile the sublimation zone was heated up to 155°C; then 70 ml/min of Ar flow though sublimation zone delivered $Co(acac)_2$ to the deposition zone. The total flow rate through deposition zone during CVD of Co was 100 ml/min; 70 ml/min of Ar carrying $Co(acac)_2$ and 30 ml/min H_2 through bottom inlet of CVD reactor. This flow rate was adjusted and ensured to have a bubbling fluidized flow regime in deposition zone.

The temperature of the sublimation zone was kept constant during deposition process, and the deposition of $Co(acac)_2$ on CeO_2 and Pt/CeO_2 was studied at the temperature range of 150 – 180°C to obtain preferential CVD condition of $Co(acac)_2$ on platinum surface. The concentration of Acetylacetone (Hacac) as the main product of CVD reaction was monitored by Pfeiffer Omnistar GSD 300 02 Mass Spectrometer using electron emission ionizer and Quadrupole – Channeltron detector. The concentration change of Hacac in outlet of CVD reactor was also monitored using a BRUKER vector 22 FT-IR spectrometer and a homemade gas cell.

Characterizations techniques

Elemental analysis

Metal loading determination was done using a Varian SpectrAA 220FS double beam atomic absorption spectrometer fitted with standard 37 mm hollow cathode lamps for Co and Pt. Measurements were done using an acetylene/air burner. Samples were digested in a reverse aquaregia and subsequently diluted by the Milli-Q water. The standard solutions for instrument calibration were purchased from Acros with 1000 ppm of metallic cations, and for each element 5 calibration solutions were prepared in concentration range of 0 to 30 µg/ml for Co and 0 to 90 µg/ml for Pt.

Powder X-ray diffraction

X-ray diffraction (XRD) of samples was recorded using D8 Advance Bruker Bragg-Brentano diffractometer operating at 45 kV, 40 mA with Cu Kα ($\lambda = 1.541$ Å) radiation and utilizing a LYNXEYE XE high-resolution energy dispersive 1D detector. The in-situ XRD patterns were recorded using the XRK 900 Anton Paar reactor chamber. The in situ measurement was carried out under hydrogen flow with the heating rate of 5°C/min up to 650°C in 2θ range of 37.5 – 42.5° with step size of 0.001° and accumulation time of 5 sec/step.

High resolution electron microscopy

The HR-STEM pictures were captured using a Hitachi HD-2700CS electron microscope with a cold field emission gun operated at 200 kV and high-angle annular dark field detector (HAADF-STEM, Z contrast). Also a secondary electron detector was used to obtain SEM images. The average particle size and particle size distribution histograms were obtained considering 100 NPs randomly.

Fourier transform infrared spectroscopy

The CO adsorption on Pt/CeO_2 and Pt_3Co/CeO_2 was investigated using the NICOLET iS50 FT-IR spectrometer. A custom made operando cell[4] was used for pretreatment and CO adsorption study. After high temperature annealing, the sample was grinded and pelletized, then reduced at 400°C for 4 h under 20 ml/min flow of H_2 with heating rate of 5°C/min. After cooling down to room temperature and purging with He, CO was introduced to the chamber for 10 min followed by purging with He again. After removing gas phase and physically adsorbed CO, (10 min purging), the spectrum was collected.

BET surface area measurement

BET surface area and pore characteristics of samples were measured by nitrogen physisorption at 77 K using a 3Flex physisorption and chemisorption instrument (Micromeritics). The samples were degassed at 300 °C under vacuum for 24 h.

X-ray absorption spectroscopy

Co *K* and Pt L_3 XAS spectra were measured at the SuperXAS beamline[5] at the Swiss Light Source (Paul Scherrer Institute, Villigen, Switzerland). The incident beam was provided by a 2.9 T super-bend magnet. The SLS was running in the standard top-up mode at 2.4 GeV and with an average current of 400 mA. The Si surface of a collimating mirror at 2.8 mrad was used for harmonic rejection at Co *K* edge. For Pt L_3 edge XAS we used the Rh-coated surface of the collimation mirror at 2.8 mrad. Energy was selected by a Si(111) channel cut monochromator. The beam was focused down to 0.1 mm in vertical direction and 0.3 mm in horizontal direction by a Rh coated toroidal mirror. The photon flux obtained at the sample was about 5×10^{11} photons/s at the Co *K* edge and 8×10^{11} photons/s at the Pt L_3 edge. The energy was calibrated using standard Co and Pt foils. The sample was sealed under inert atmosphere in quartz capillaries (1 mm OD, 0.01 mm), the oxygen concentration was below 0.2 ppm during sample transfer to capillary. The XAS spectra were collected in fluorescence mode using 5-element silicon drift detector. We processed the spectra using IFEFFIT software package[6]. We fitted the EXAFS spectra for cobalt and platinum simultaneously. The So2 parameters were calculated using EXAFS spectra Co and Pt reference foils and fixed at 0.74 and 0.86, respectively. The EXAFS at Co *K*-edge were fit in R space with K-weighting of 3 in the range of k=3-12 Å^{-1} with dk=0.5 and R=1-3 Å with dR=1. At Pt L_3 edge we fit EXAFS in R space with k-weighting of 3 in the range of k=3-12 Å^{-1} with dk=0.5 and R=1.3-3.5 Å with dR=1. The scattering paths were generated using metallic Co and Pt_3Co reference structures. We fixed the Debye-Waller factor for all coordination shells to the same value and made a constrain $N_{Co\text{-}Pt} = 3\times N_{Pt\text{-}Co}$ based on Pt to Co ratio of 3.

Evaluation of catalytic activity

Preferential oxidation of carbon monoxide (CO PROX) were carried out in an atmospheric tubular quartz reactor (OD: 6mm, ID: 4 mm). Typically 100 mg of catalyst was diluted with 300 mg of silicon carbide (SiC) powder and located in the reactor. A mixture of CO (1%), O_2 (1%), H_2 (40%), and Ar (balance) was used as reactant gas. Prior to the reaction, the catalyst was reduced and annealed under pure hydrogen flow at 550°C for 6 h with heating rate of 5°C/min. After cooling to room temperature, the ultra-active sites were killed using 50 ml/min of reactant gas for 30 min and purging with Ar. The sample were relaxed overnight, then the CO PROX reaction was carried out starting from room temperature and total flow of 50 ml/min. The reaction temperature was increased stepwise and the products were analyzed using an INFICON micro GC 3000. The CO_2 selectivity was calculated based on total amount of O_2 used for CO_2 formation ($S_{CO_2} = n_{CO_2}/2\left[n_{O_2in} - n_{O_2out}\right]$).

Computational details

All ground-state total energy calculations in this work have been performed with the all-electron full-potential DFT code FHI-aims.[7, 8] Electronic exchange and correlation was treated on the hybrid functional level with the PBE0 functional.[9] All geometry optimization were done with the "tier2" atom-centered basis set using "tight" settings for numerical integrations. Local structure optimization is done using the Broyden-Fletcher-Goldfarb-Shanno method[10] relaxing all force components to smaller than 10^{-2} eV/Å.

The Nudged Elastic Band (NEB)[11] method as implemented in the ASE[12] package was used to find the transition paths and corresponding energy barriers between given initial and final states, which were defined as the locally optimised structures of adjacent reaction intermediates. A chain of six replicas of the system has been constructed for every transition state calculation, and the forces were allowed to relax with a threshold of 0.05 eV/Å. The two states are assumed to be connected by a single barrier path.

All molecular dynamics (MD) simulations have been carried out using the DL_POLY package.[13] All cluster systems have been simulated for 10 ns with additional, 1 ns used for equilibration. The Gupta potential[14] was used to model the interactions between atoms. The general form of the Gupta potential reads as:

$$U_{tot} = A\sum_{j \neq i}^{N} v(r_{ij}) - \xi \sum_{i=1}^{N} \sqrt{\rho(r_i)},$$

where the potential $\upsilon(r_{ij})$ is pairwise and defined as:

$$v(r_{ij}) = exp\left[- p\left(\frac{r_{ij}}{r_0} - 1\right)\right],$$

and the function $\rho(r_i)$ is given by:

$$\rho(r_i) = \sum_{j \neq i}^{N} exp\left[- 2q\left(\frac{r_{ij}}{r_0} - 1\right)\right],$$

where A, ξ, p, r_0, and q_0 are potential parameters. The values used in this study were taken from Ref.[15] and are summarized in Table X.

Table S-1. Gupta potential parameters for Co–Pt nanoalloys

	Co-Pt parameters [15]				
	A/eV	ξ/eV	p_{ij}	q_{ij}	r_0/Å
Pt-Pt	0.242	2.506	11.140	3.680	2.770
Pt-Co	0.245	2.386	9.970	3.320	2.590
Co-Co	0.189	1.907	8.800	2.960	2.500

The Velocity Verlet algorithm[16] was used to integrate the equations of motion in the NVT ensemble. The length of time step was chosen as 1 fs. The Nosé-Hoover thermostat[17, 18] with relaxation time of 0.01 ps was used to conserve the temperature.

Figure S-2:

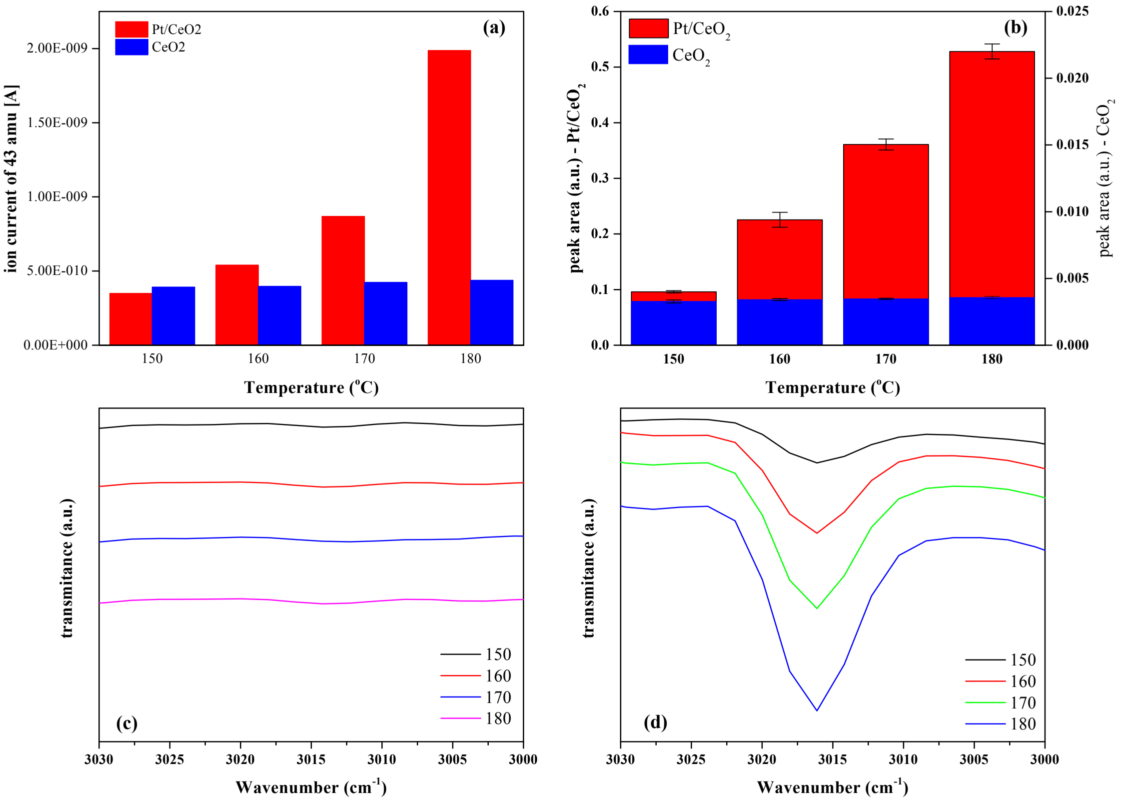

Fig. S-2. The ion current plot of Hacac, 43 amu (a), peak area of 3015 cm^{-1} (the error bars show corresponding standard deviations) (b), FT-IR spectrum in range of 3000 to 3030 cm^{-1} during Co(acac)$_2$ CVD on CeO$_2$ (c) and Pt/CeO$_2$ (d) in different temperatures.

Figure S-3:

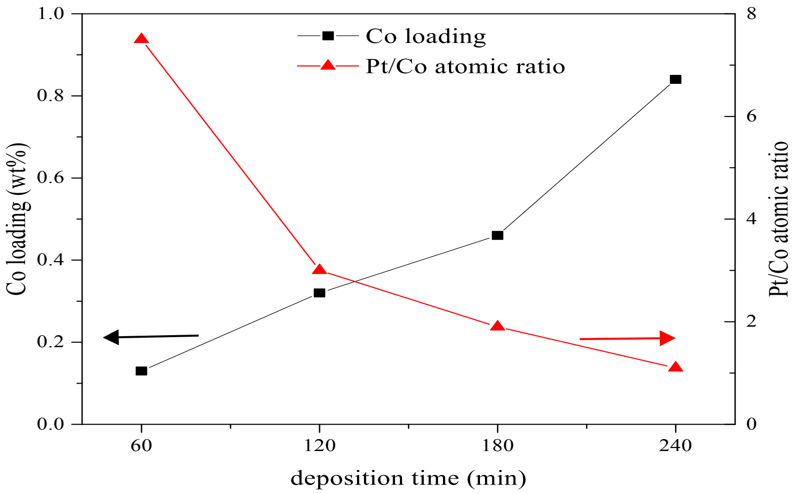

Fig. S-3. The cobalt loading and Co to Pt atomic ratio of different Co-Pt/CeO_2 samples synthesized by PCVD method as a function of deposition time.

Figure S-4:

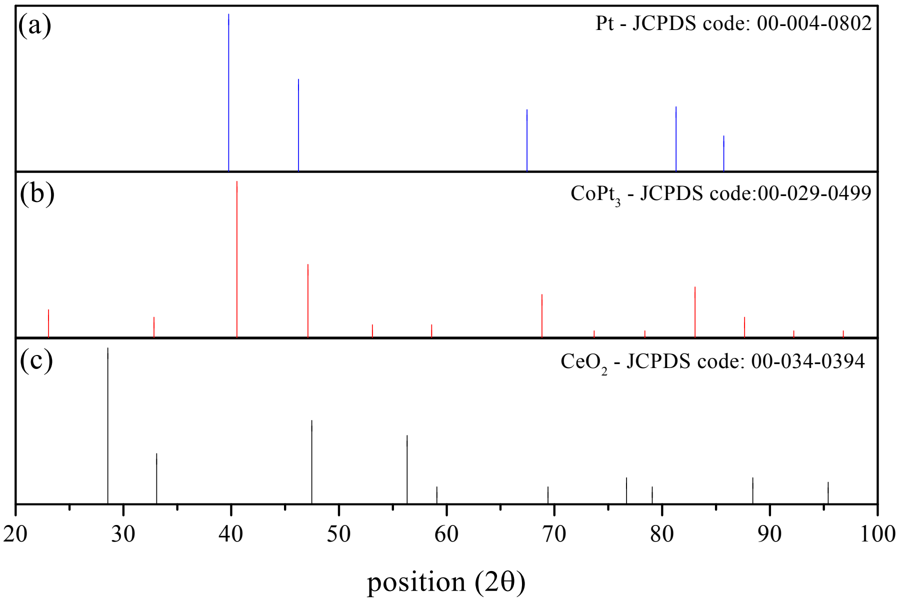

Fig. S-4. Reference XRD patterns of (a) Pt, (b) Pt_3Co, and (c) CeO_2.

Figure S-5:

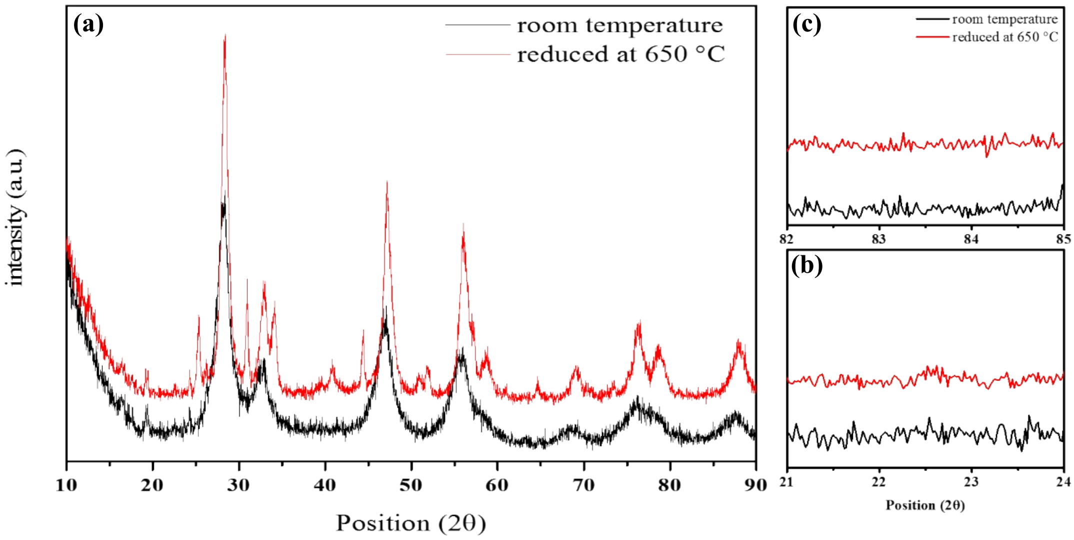

Fig. S-5. In-situ XRD pattern of $CoPt_3/CeO_2$-CVD sample during reduction course; whole spectrum (a), and magnified spectrum in range of 21° - 24° (b) and 82° - 85° (c).

Figure S-6:

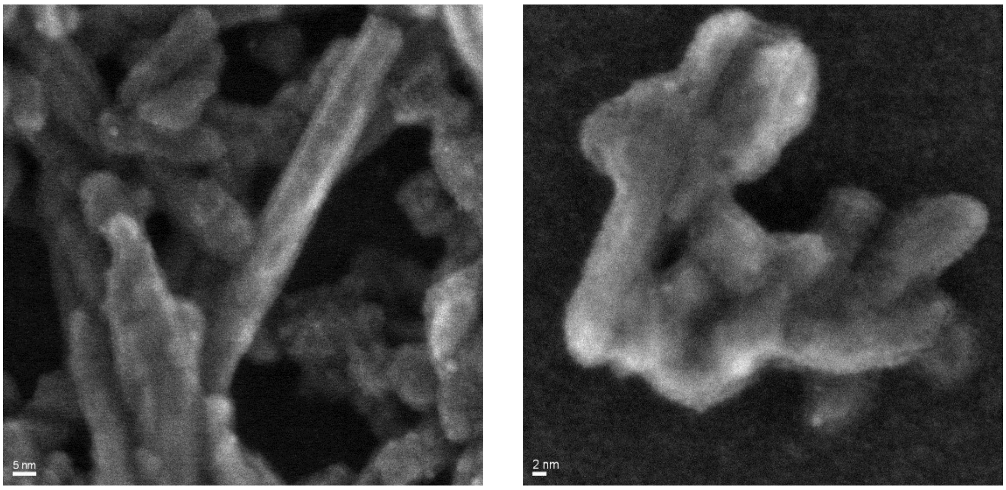

Fig. S-6. SEM image of Pt_3Co/CeO_2-CVD sample.

Figure S-7:

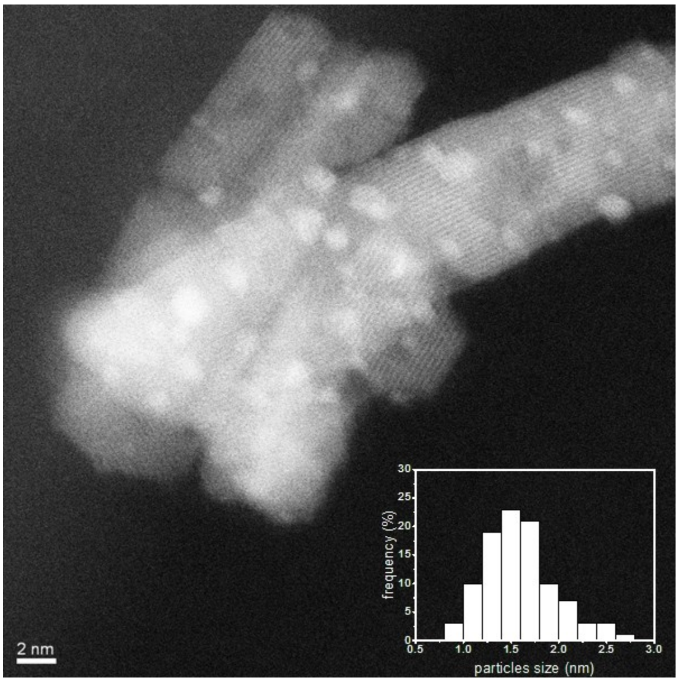

Fig. S-7. HAADF-STEM images and particles size distribution histogram (inset) of Co-Pt/CeO_2-CVD sample with Co to Pt ratio of 1/3 synthesized with successive impregnation, annealed at 550°C for 6 h.

Figure S-8:

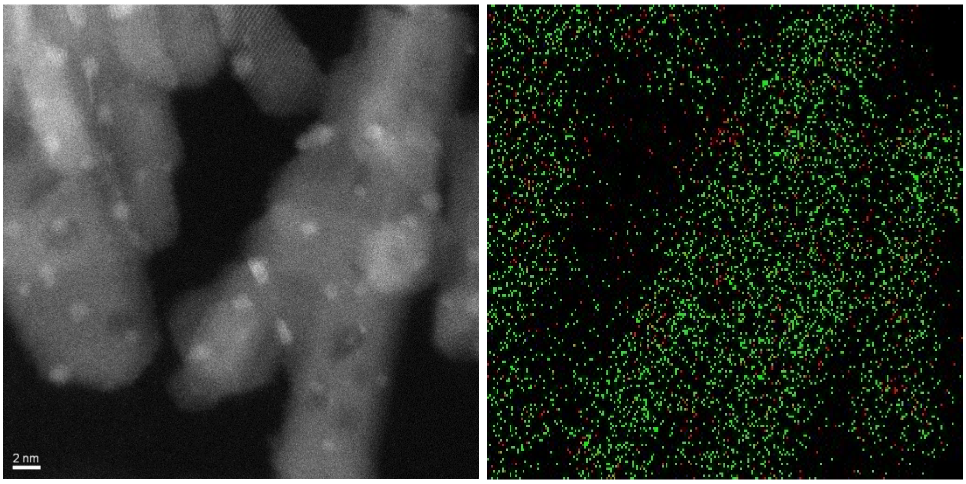

Fig. S-8. STEM image and elemental mapping of $CoPt_3$/CeO_2-CVD sample. The elements are marked with color dots as: Ce (green), Co (blue), and Pt (red).

Figure S-9:

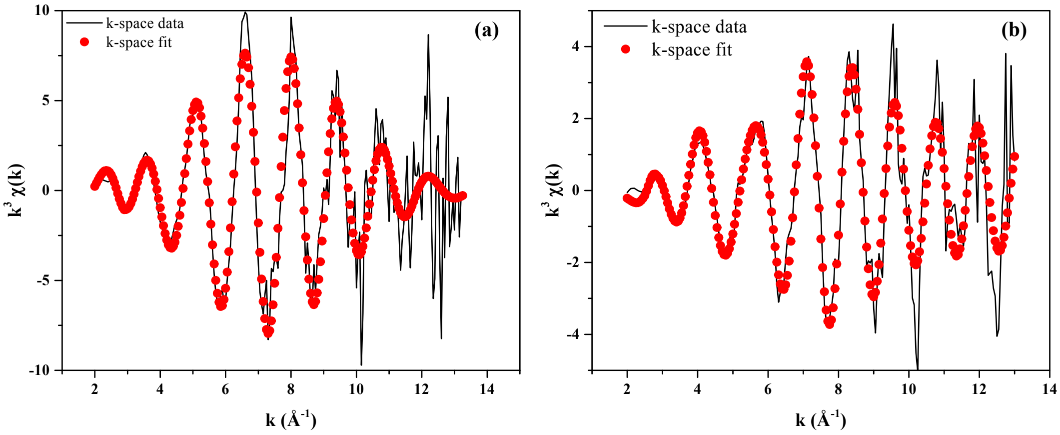

Fig. S-9. k-space data and fit of (a) Co K edge and (b) Pt L_3 edge of Pt_3Co/CeO_2-CVD sample.

Figure S-10:

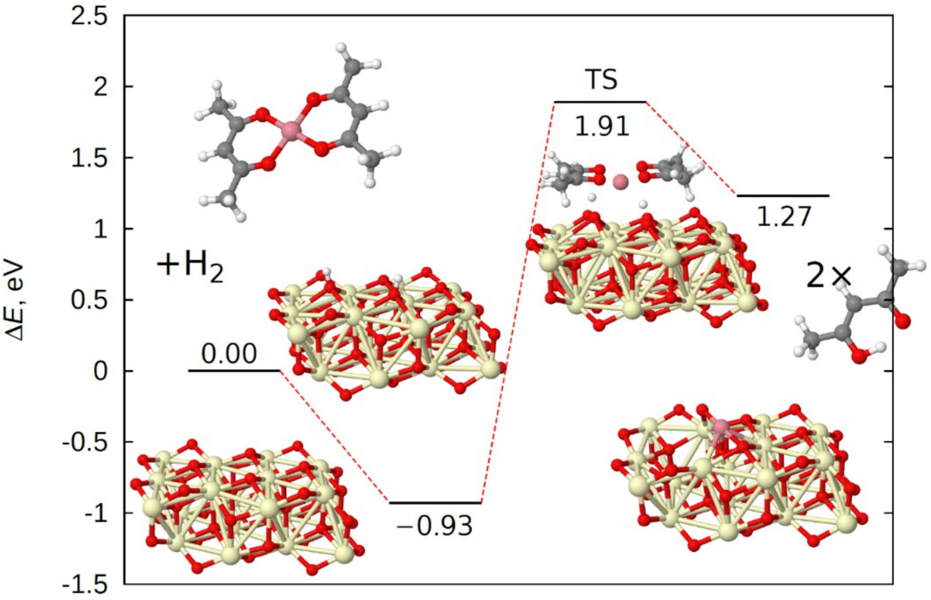

Fig. S-10. Reaction profile of $Co(acac)_2$ reduction on CeO_2 (111).

Figure S-11:

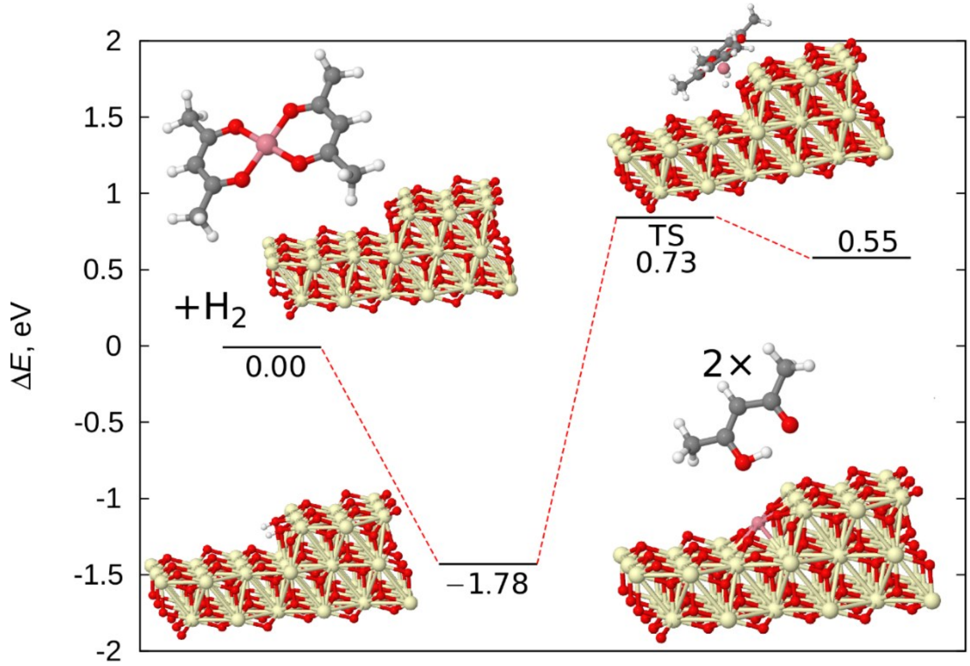

Fig. S-11. Reaction profile of Co(acac)$_2$ reduction on stepped CeO$_2$ (111).

Figure S-12:

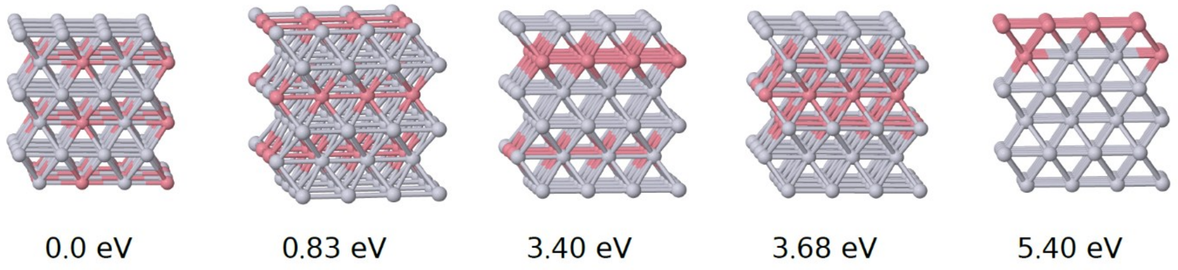

Fig. S-12. Relative thermodynamic stabilities of different Pt$_3$Co phases.

Figure S-13:

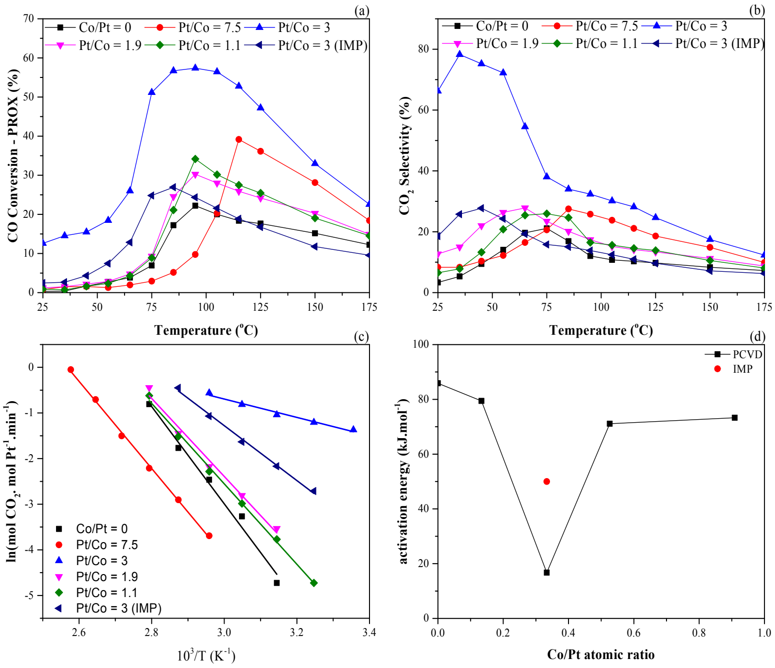

Fig. S-13. Comparison of catalytic activity of Co-Pt/CeO$_2$-PCVD samples with different Co to Pt ratios and Pt$_3$Co/CeO$_2$-IMP sample in CO PROX. CO conversion (a), CO$_2$ selectivity (b), Arrhenius plot of CO PROX rate (c), and activation energies of CO$_2$ formation (d). The singular red point presents the obtained activation energy for IMP sample.

Table S-2:

Table S-2. BET surface area of main samples.

Sample	BET surface area (m$_2$/g)	BJH cumulative pore volume (cm^3/g)^a	BJH average pore width (Å)^b
CeO$_2$	123	0.462	179
Pt/CeO$_2$	117	0.384	155
Pt$_3$Co/CeO$_2$-CVD	89	0.277	150
Pt$_3$Co/CeO$_2$-IMP	79	0.269	156

Table note:

a) This value shows the BJH Adsorption cumulative surface area of pores.
b) This value shows the BJH Adsorption average pore width.

Table S-3:

Table S-3. Comparison of recently developed platinum based bimetallic alloyed catalysts for CO PROX.

Catalyst[a]	Synthesis method	Pt loading (wt %)	Max conversion (%)[b]	Max conversion Temp. (°C)[c]	Catalysis condition[d]	Reference
Pt/γ -Al_2O_3	incipient wetness impregnation	2	40	250	50 mg, 200 ml/min	19
Pt/CeO_2	wet impregnation	5	59	110	73 mg, 100 ml/min	20
$PtCu/SiO_2$	successive impregnation	3	70	130	50 mg, 140 ml/min	21
Pt_3Co/SiO_2	pore-filling	3	90	150		
$PtAu/CeO_2$	sol impregnation	0.5	90	80	100 mg, 50 ml/min	22
$PtCu/\gamma$-Fe_2O_3	electron beam irradiation	2.9	68	100	50 mg, 25 ml	23
$PtCu/CeO_2$	electron beam irradiation	2.5	57	100		
PtPd/ZnO	liquid phase reduction	1	90	180	100 mg, 60 ml/min	24
$PtCo/CeO_2$	incipient wetness impregnation	3.85	66	110	50 mg, 230 ml/min	25
$PtCo/\gamma$-Al_2O_3	incipient wetness impregnation	3.85	93	100		
$PtCu/\gamma$-Al_2O_3	radiolytic process	7.5	38	120	50 mg, 25 ml	26
Pt-Fe Alloy@SiO_2	alloying–dealloying process	3.1	46	90	20 mg, 30 ml	27
$PtCu/Al_2O_3$	liquid-phase reductive deposition	3.0	96	140	50 mg, 140 ml/min	28
Pt_3Co/CeO_2	successive impregnation	3.0	27	85	100 mg, 50 ml/min	current study
Pt_3Co/CeO_2	PCVD	3.0	57	85		

Table note:

a) The reported bimetallic catalysts are in alloy form.
b) The catalytic activity data of different works summarized in this table are not fairly comparable due to different preparation methods, reaction conditions, and support type.
c) These data present the temperature of maximum CO conversion in PROX reaction.
d) The data in this column present the amount of used catalyst (mg) and flow rate (ml/min) of the feed gas used in catalysis. However, the composition of feed gas is not same.

References

1. H.-X. Mai, L.-D. Sun, Y.-W. Zhang, R. Si, W. Feng, H.-P. Zhang, H.-C. Liu and C.-H. Yan, *The Journal of Physical Chemistry B*, 2005, **109**, 24380-24385.
2. M. J. Parnian, A. A. Khodadadi, A. Taheri Najafabadi and Y. Mortazavi, *Applied Catalysis A: General*, 2014, **470**, 221-231.
3. A. Taheri Najafabadi, A. A. Khodadadi, M. J. Parnian and Y. Mortazavi, *Applied Catalysis A: General*, 2016, **511**, 31-46.
4. S. B. Rasmussen, S. Perez-Ferreras, M. A. Bañares, P. Bazin and M. Daturi, *ACS Catalysis*, 2013, **3**, 86-94.
5. P. M. Abdala, O. V. Safonova, G. Wiker, W. V. Beek, H. Emerich, J. A. V. Bokhoven, J. Sá, J. Szlachetko and M. Nachtegaal, *Chimia*, 2012, **66**, 699-705.
6. M. Newville, *Journal of Synchrotron Radiation*, 2001, **8**, 322-324.
7. V. Blum, R. Gehrke, F. Hanke, P. Havu, V. Havu, X. Ren, K. Reuter and M. Scheffler, *Computer Physics Communications*, 2009, **180**, 2175-2196.

8. R. Xinguo, R. Patrick, B. Volker, W. Jürgen, T. Alexandre, S. Andrea, R. Karsten and S. Matthias, *New Journal of Physics*, 2012, **14**, 053020.
9. C. Adamo and V. Barone, *The Journal of Chemical Physics*, 1999, **110**, 6158-6170.
10. in *Numerical Optimization*, Springer New York, New York, NY, 2006, DOI: 10.1007/978-0-387-40065-5_15, pp. 421-447.
11. G. Henkelman, B. P. Uberuaga and H. Jónsson, *The Journal of Chemical Physics*, 2000, **113**, 9901-9904.
12. S. R. Bahn and K. W. Jacobsen, *Computing in Science and Engineering*, 2002, **4**, 56-66.
13. I. T. Todorov, W. Smith, K. Trachenko and M. T. Dove, *Journal of Materials Chemistry*, 2006, **16**, 1911-1918.
14. R. P. Gupta, *Physical Review B*, 1981, **23**, 6265-6270.
15. C. Goyhenex, H. Bulou, J. P. Deville and G. Tréglia, *Physical Review B*, 1999, **60**, 2781-2788.
16. W. C. Swope, H. C. Andersen, P. H. Berens and K. R. Wilson, *The Journal of Chemical Physics*, 1982, **76**, 637-649.
17. S. Nosé, *The Journal of Chemical Physics*, 1984, **81**, 511-519.
18. W. G. Hoover, *Physical Review A*, 1985, **31**, 1695-1697.
19. B. Atalik and D. Uner, *Journal of Catalysis*, 2006, **241**, 268-275.
20. O. Pozdnyakova, D. Teschner, A. Wootsch, J. Kröhnert, B. Steinhauer, H. Sauer, L. Toth, F. C. Jentoft, A. Knop-Gericke, Z. Paál and R. Schlögl, *Journal of Catalysis*, 2006, **237**, 1-16.
21. T. Komatsu and A. Tamura, *Journal of Catalysis*, 2008, **258**, 306-314.
22. Y. Liu, B. Liu, Y. Liu, Q. Wang, W. Hu, P. Jing, L. Liu, S. Yu and J. Zhang, *Applied Catalysis B: Environmental*, 2013, **142**, 615-625.
23. J. Kugai, T. Moriya, S. Seino, T. Nakagawa, Y. Ohkubo, H. Nitani, Y. Mizukoshi and T. A. Yamamoto, *Applied Catalysis B: Environmental*, 2012, **126**, 306-314.
24. H. Zhang, M. Jin, H. Liu, J. Wang, M. J. Kim, D. Yang, Z. Xie, J. Liu and Y. Xia, *ACS Nano*, 2011, **5**, 8212-8222.
25. D. I. Potemkin, E. Y. Filatov, A. V. Zadesenets, P. V. Snytnikov, Y. V. Shubin and V. A. Sobyanin, *Chemical Engineering Journal*, 2012, **207**, 683-689.
26. J. Kugai, R. Kitagawa, S. Seino, T. Nakagawa, Y. Ohkubo, H. Nitani, H. Daimon and T. A. Yamamoto, *Applied Catalysis A: General*, 2011, **406**, 43-50.
27. H. Zhao, D. Wang, C. Gao, H. Liu, L. Han and Y. Yin, *Journal of Materials Chemistry A*, 2016, **4**, 1366-1372.
28. T. Komatsu, M. Takasaki, K. Ozawa, S. Furukawa and A. Muramatsu, *The Journal of Physical Chemistry C*, 2013, **117**, 10483-10491.